Photon and π^0 separation by shower shape analysis in the Forward Calorimeter

Gordian Zomer
Supervisor: dr. ir. M. van Leeuwen
University of Utrecht

August 12, 2013

Abstract

Simulations were done to research single photon and π^0 separation in the Forward Calorimeter, which is proposed as an upgrade for ALICE at CERN. Photons from π^0 decay form background radiation for direct photon detection. In order to reject the background, the particle reconstruction needs to identify the particles correctly. Research on the cluster sizes is done to analyze the clusters left behind by single photons and π^0 decay photons in the detector. To do this logarithmic weighting is used. The best value for the logarithmic weighting parameter w_0 was $w_0 \backsimeq 5.8$.

Contents

1 Introduction

Subatomic physics deals with entities smaller that the atom. The research done in this branch of physics involves understanding the basic building blocks of matter and the forces that act on them. In everyday life the only forces we notice are gravitation and electromagnetism. On subatomic length scales (order of 10^{-15} m), however, the strong and the weak are introduced and the gravitational force is neglected, leaving three forces to be considered. The strong and the weak force vanish at atomic and larger distances. The strong force holds nuclei together, with a very short range. The weak force has an even shorter range of interaction.

To describe interactions at subatomic length scales quantum mechanics and quantum field theory have been invented. Part of this is Quantum Electro Dynamics (QED) and Quantum Chromo Dynamics (QCD). QED is relatively well understood and it explains the electromagnetic interactions between photons and charged particles. QCD describes the interactions between quarks and gluons that interact via the strong force. QCD as the general theory is considered to be complete, only it is a much more complicated theory and most of the problems are not yet solved, implying that some qualitative features (like confinement) can not be directly derived from the theory. The weak interaction is described together with the electromagnetic interaction in a unified, so-called electro-weak theory and it allows quarks to change their 'flavour'.

To study the forces and particles at these small length scales, particle accelerators are constructed. The scattering experiments that are done with accelerators allow a glimpse at the structure of the smallest particles. The Large Hadron Collider (LHC) at CERN is todays largest particle accelerator, which yields the highest energy collisions. One of the largest experiments at CERN is ALICE (A large Ion Collider Experiment). As the name suggest, ALICE is optimized to study heavy ion collisions, such as Pb-Pb.

The Forward Calorimeter (FoCal) is proposed as an upgrade of the ALICE detector. Among others, it will be used to detect direct photons from the collisions. These photons provide hints of what happens during the collisions. The collisions also generate a large amount of π^0 particles, which decay into photons. These π^0 decay photons are considered to be background radiation that interferes with the direct photon measurements. In order to know what photons are direct photons from the collisions, the π^0 decay photons need to be filtered out.

The main goal of this research is to be able to differentiate between single photons, and photons coming from π^0 decay, in order to filter π^0 decay photons. There are multiple ways to do this: first, FoCal will use a clustering algorithm that can identify hits of photons in the detector and is able through the invariant mass, to reconstruct the mother particle, such as the π^0. This only works when two clusters of photons that overlap only slightly or not at all. When two clusters do overlap a second method might be used: shower shape reconstruction, which uses the widths of a cluster to determine whether the incoming particle was a single photon or were perhaps two photons.

In order to understand what happens at π^0 decay, a bit of theory is spent on explaining photon detection and on kinematics. After that FoCal specific information will be given, followed by the simulations for this research and their results.

2 Theory

If we want to detect direct photons from the collisions we need to remove the background caused by π^0 decay. To do this, it is good to know about how photons are being detected and what the influence of π^0 decay actually is. Also the definitions of *radiation length* and *Molière radius* are useful concepts.

2.1 Photon detection

In order to detect photons, a calorimeter can be used. A calorimeter is a device that stops incoming particles and it has properties to identify the particle's energy. There are two types of calorimeters: electromagnetic and hadronic. Electromagnetic calorimeters are designed mainly to detect the energy of particles that interact electromagnetically. Hadronic calorimeters are used when hadronic interactions play a bigger part.

A calorimeter is usually designed to completely stop or absorb the particles. In this way the particles (are forced to) deposit all of their energy. Calorimeters usually consist of two types of materials: a high density absorber interleaved with an active material. The absorber converts the particles into showers of more particles with lower energy. The active material is for example silicon which acts as an electronic sensor.

2.2 π^0 decay

In $p+p$ and $p+A$ collisions lots of π^0 are created. The decay of a π^0 is as follows: $\pi^0 \to \gamma\gamma$. If we want to remove the background formed by these π^0 decay photons we need to understand their kinematics. We are interested in direct photons at forward rapidities, so π^0 at forward rapidities will also be measured. In the following sections π^0 kinematics and the reconstruction through their invariant mass will be explained.

2.2.1 Relativistic kinematics

The mean life time of a π^0 in the lab frame is about 10^{-17} s. The speed is relativistic (near c), so in the lab frame the distance x they travel before decaying is approximated by $x = c * 10^{-17}\text{s} \backsimeq 10^{-9}$ m, which is about 1 nanometer.

In its rest frame the decay products of a π^0 are always back to back, see Fig. 1a. If we want to transform this to the lab frame, we need to use a bit of special relativity. Here, natural units are used, so $c = 1$.

The momentum for a particle is given as a four-vector:

$$p = \begin{pmatrix} E \\ p_x \\ p_y \\ p_z \end{pmatrix},$$

with p_x, p_y and p_z the momenta in the x-, y- and z-directions and E the energy of the particle. For special relativity the Minkowski metric is used. With this metric an inner product of two four-vectors p_1 and p_2 is done as follows:

$$\begin{aligned} p_1.p_2 &= (E_1, p_{x,1}, p_{y,1}, p_{z,1}) \begin{pmatrix} 1 & 0 & 0 & 0 \\ 0 & -1 & 0 & 0 \\ 0 & 0 & -1 & 0 \\ 0 & 0 & 0 & -1 \end{pmatrix} \begin{pmatrix} E_2 \\ p_{x,2} \\ p_{y,2} \\ p_{z,2} \end{pmatrix} \\ &= E_1 E_2 - (p_{x,1}p_{x,2} + p_{y,1}p_{y,2} + p_{z,1}p_{z,2}) \ . \end{aligned} \tag{1}$$

Now we want to do a Lorentz transformation from S to $S^{'}$, with $S^{'}$ moving at constant velocity v in the x-direction with respect to S.

$$p' = \begin{pmatrix} \gamma & -\gamma\beta & 0 & 0 \\ -\gamma\beta & \gamma & 0 & 0 \\ 0 & 0 & 1 & 0 \\ 0 & 0 & 0 & 1 \end{pmatrix} p \tag{2}$$

This is true for any four-vector. p is the four-vector in S, p' is the four-vector in S', β is the velocity v in units of c and γ is defined as:

$$\gamma = \frac{1}{\sqrt{1-\beta^2}} \ . \tag{3}$$

Such an inner product in the Minkowski metric is called *Lorent invariant*, because it does not change under a Lorentz transformation. This means that $p_1.p_2 = p'_1.p'_2$.

To illustrate we now want to do a Lorentz transformation on the rest frame in Fig. 1a. This results in Fig. 1b, where θ_{b1} is the angle of photon 1 with the horizontal axis *before* the Lorentz transformation and θ_{a1} is the angle of photon 1 *after* the Lorentz transformation. The same goes

for photon 2. In the figures it is visible that the photons are boosted in the z-direction in the lab frame. This is also refered to as a *Lorentz boost*.

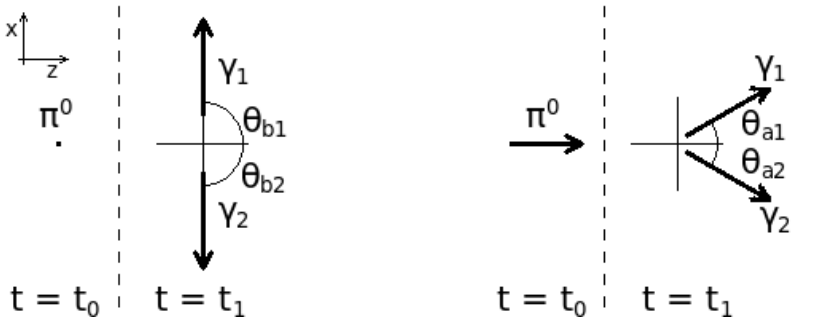

(a) π^0 in its rest frame.

(b) π^0 in lab frame traveling in $\hat{z}$-direction.

Figure 1: Photon momentum *before* and *after* Lorentz boosting. In this example photons decay perpendicular to the π^0 momentum and are then Lorentz boosted. $\theta_{b1} = -\theta_{b2}$ and $\theta_{a1} = -\theta_{a2}$.

Fig. 2a is a different case, where photon 1 decays at an angle $\theta_{b1} < 90°$ with the z-axis. This has the results that photon 1 gets a higher momentum in the z-direction than photon 2, because photon 1 already has a larger momentum in the positive z-direction than photon 2, before the Lorentz transformation.

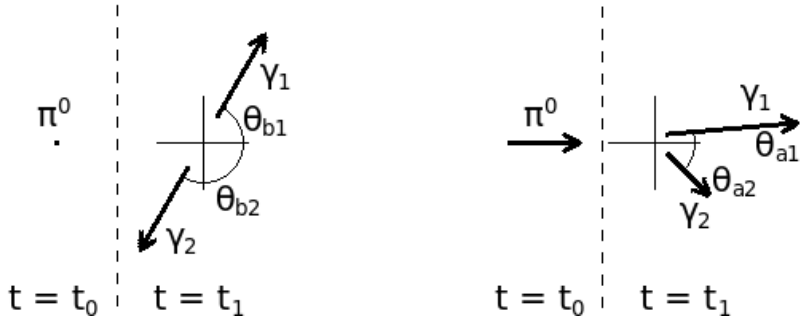

(a) π^0 in its rest frame.

(b) π^0 in lab frame traveling in $\hat{z}$ direction.

Figure 2: Photon momentum *before* and *after* Lorentz boosting. Photon 1 decays at an angle $\theta < 90^\circ$ and photon 2 decays at an angle $180^\circ + \theta$ to the π_0 momentum and they are then Lorentz boosted.

2.2.2 Invariant mass

For the invariant mass calculation, natural units are also used. First we have the relativistic energy:

$$E^2 = m^2 + p^2 \,, \tag{4}$$

with m the rest mass and p the momentum.

The rest mass of photons is zero, therefore photon momentum and energy are the same in natural units,

$$E_\gamma^2 = p_\gamma^2 \,. \tag{5}$$

The invariant mass m_{12} is given by:

$$m_{12} = \sqrt{(E_1 + E_2)^2 - \left(\vec{p_1} + \vec{p_2}\right)^2} \tag{6}$$

$$m_{12} = \sqrt{E_1^2 + E_2^2 + 2E_1E_2 - p_1^2 - p_2^2 - 2\vec{p_1}.\vec{p_2}} \,. \tag{7}$$

Filling in $p_i^2 = E_i^2$ yields:

$$m_{12} = \sqrt{2E_1E_2 - 2\vec{p_1}.\vec{p_2}} \,. \tag{8}$$

Working out the inner product:

$$\vec{p_1}.\vec{p_2} = \left|\vec{p_1}\right| \left|\vec{p_2}\right| \cos(\theta_{12}) = E_1E_2 \cos(\theta_{12}) \tag{9}$$

$$m_{12} = \sqrt{2E_1E_2 - 2E_1E_2\cos(\theta_{12})} = \sqrt{2E_1E_2\,(1 - \cos(\theta_{12}))}, \tag{10}$$

with θ_{12} the angle between the two photons, $\theta_{12} = |\theta_{a1}| + |\theta_{a2}|$ in Fig. 1 and Fig. 2. Please note that the above expression is only valid for photons, since their rest mass is zero.

In the experiment E_1, E_2 and the photon positions and angles are measured. One can now easily obtain the invariant mass of the mother particle. The determination of the energy of the clusters will require some work as will be discussed later on.

From Eq. (10) we know the invariant mass m_{12} as a function of θ. Rewriting this equation to have θ as a function of m_{12} yields the following:

$$\theta = \arccos\left(\frac{2E_1E_2 - m_{12}}{2E_1E_2}\right). \tag{11}$$

There are three limit cases:

$$\begin{aligned} 2E_1E_2 \gg m_{12} &\Rightarrow \theta \to 0 \\ 2E_1E_2 = m_{12} &\Rightarrow \theta = \frac{\pi}{2} \\ 2E_1E_2 \ll m_{12} &\Rightarrow \theta \to \pi, \end{aligned}$$

with m_{12} of course the π^0 rest mass and E_1 and E_2 the energy of the first and second decay photon. Thus when the photons have high energy compared to the rest energy of the π^0, the angle will be very small. This is the case when the decaying π^0 had a high momentum. The goal of this research is to optimize parameters to find a difference between single photon clusters and clusters of two photons coming from π^0. The clusters of the π^0 decay photons are very close together if the opening angle is very small.

2.3 Radiation length

When a high-energy photon hits a dense absorber (like tungsten or lead) it generates an electromagnetic cascade or shower. The photon generates electrons and positrons through pair production, which in turn generate photons of lower energy due to bremsstrahlung. This process continues until the electrons reach a certain critical energy and then dissipate their energy through ionization and excitation of the absorber instead of the generation of new shower particles. The longitudinal development of the shower is caused by the high-energy part of the shower.

The radiation length X_0 (usually in g/cm^2) is a quantity that describes the longitudinal profile of an electromagnetic cascade; it is a characteristic length of the amount of matter traversed in which pair production or bremsstrahlung occurs, for photons and electrons respectively. For photons, this X_0 is $\frac{7}{9}$ of the mean free path for pair production. For electrons it is the mean distance for which the fraction of the energy that is left is $\frac{1}{e}$, while the rest of the energy is dissipated by bremsstrahlung.

2.4 Molière radius

The Molière radius R_M of a shower is defined as the radius of the cilinder around photon direction which contains 90% of the deposited energy of a shower. Usually about 99% of this deposited energy lies within 3.5 R_M [3]. Beyond this radius the scaling with R_M fails. The showers begin with a narrow core and as it develops the core broadens.

3 FoCal

The Forward Calorimeter (FoCal) is proposed as an upgrade of the ALICE detector. ALICE was designed to study the properties of hot and dense partonic matter and FoCal will extend these capabilities to study cold dense partonic matter. FoCal will be able to provide high precision measurements of direct photons in $p+p$ and $p+A$ collisions. [2]

3.1 Technical details

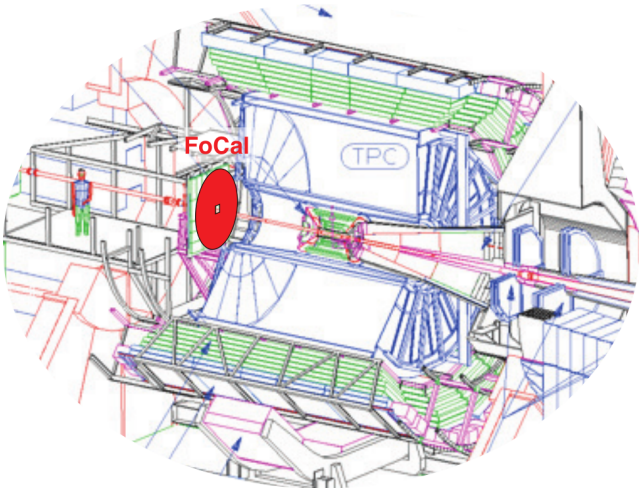

Figure 3: Proposed FoCal location in the ALICE detector

The currently proposed location of FoCal will be at 7 or 8 meters from the collision point as seen in Fig. 3. FoCal will be a disk with a thickness of 15 cm and a diameter of about 60 cm. The calorimeter will consist out of layers of tungsten interleaved with silicon layers. There will be six segments: the 1st and 3rd are the same and consist out of four layers of tungsten interleaved with low granularity (1 cm x 1 cm) silicon pads. The 5th and the 6th segment are also the same and consist out of five layers of tungsten interleaved with low granularity silicon pads. The 2nd and 4th segments consist of one layer of tungsten with a layer of high granularity (1 mm x 1 mm) silicon pixels behind it, as can be seen in Fig. 4. The difference between pads and pixels is the way they are read out by the electronics. The combination of tungsten, silicon, electronics and glue creates an effective Molière radius of about 1 cm.

In order to detect direct photons from the collisions, decay photons need to be rejected. These decay photons are mainly caused by π^0 decay. The typical opening angles of π^0 decays at forward rapidity are very small, due to the longitudinal Lorentz boost. This means that the photons coming from π^0 decay are very close together (in the order of milimeters) upon entering FoCal. Thus FoCal needs to have a high resolving power in order to separate the decay photons of π^0. To obtain this two particle separation, FoCal uses the high granularity layers in Fig. 4, which have a cell size of 1 mm x 1 mm. The segments with the coarse layers are mostly used for determining the particle energy.

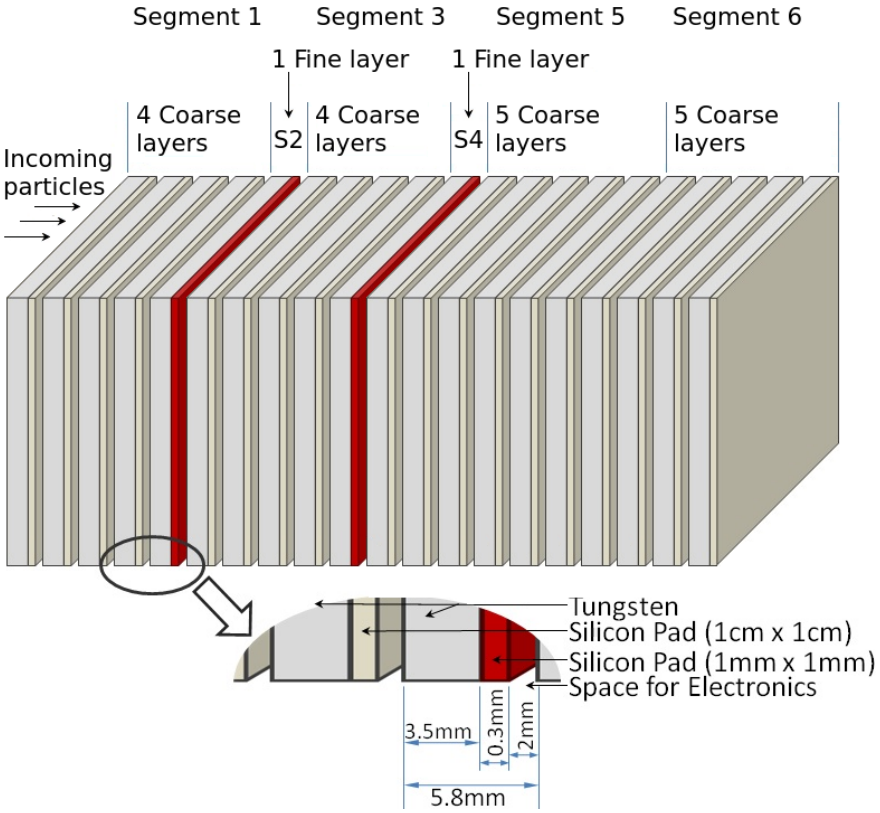

Figure 4: Schematic illustration of an ALICE FoCal module. The proposed design (LOI in 2013) has interleaved Si + W layers, with different granularity in the Si pad/pixel layers. The original image is taken from Ref. [1], but edited to resemble the detector in the LOI of 2013.

3.2 Clustering algorithm

Before building the detector, a lot of simulations have to be run to analyse how the proposed detector will respond. These simulations involve for instance direct photon and π^0 detection.

When a photon hits the detector it generates a shower. Each layer in the detector has a certain number of pixels/pads being hit. The clustering algorithm does not look at each layer, but at each segment, because the read out of the pads is also done that way. The hits in each pad per layer are summed up per segment to obtain a signal per equivalent detector cell (which is called a tower).

Per segment, the algorithm analyses the energy. It loops over all the cells (pixels or towers), beginning with the highest energy. The first energy found this way will be the highest and will be set as a possible *seed* for a cluster. Then all the cells within a certain radius will be set so that they cannot be assigned as a seed anymore (the algorithm will not be able to loop over those cells). If a significant amount of energy is found with that radius, the cell with that energy will get a certain flag, which ensures that the algorithm can loop over it. This way it can be still set as a seed. After this is done, the algorithm will check the cell with the second highest energy etc. In the end all the seeds will be checked: if a seed is found with too few cells within the cluster search radius or if a seed is found with too little energy, it will be rejected as a seed.

After all the segments have been analyzed as described above, the shower reconstruction begins. First of all, the clusters from the coarse segments will be combined. Second, the clusters from the fine segments will be combined. Now there are two lists with cluster information (one for the coarse segment clusters and one for all the fine segment clusters). Next, the algorithm analyses the clusters from the fine sections and tries to match them with the clusters from the coarse segments. When they are matched, the position information is taken from the fine segments and the energy is taken from the coarse segments. For a more elaborate explanation see Ref. [2].

4 Simulation of detector performance

When a photon hits the detector it showers and leaves energy behind. Per segment of the detector, the photon shows cluster profiles similar to Fig. 5a. The profile shown in the figure resembles a cluster in the second coarse segment of the FoCal where the width of the shower is at its maximum. Because the width of the shower at the second coarse segment is at its maximum, the cluster sizes in that segment will be the largest. The sizes of the clusters generated for this research are comparable to the sizes of the clusters in the second coarse segment in the FoCal, bacause this yields the highest discriminating power when clusters start to overlap.

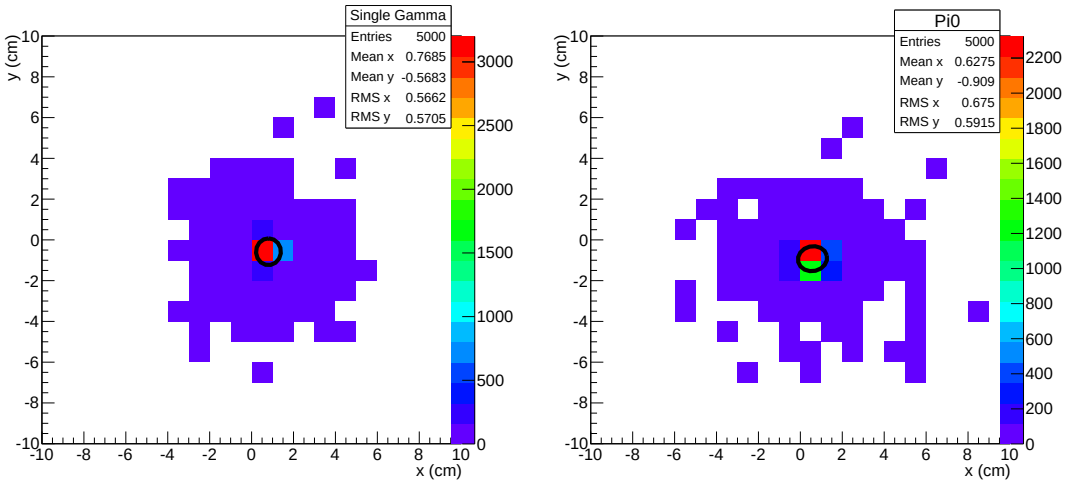

(a) Example of a profile of a simulated photon cluster.

(b) Example of a profile of simulated merged π^0 photon clusters.

Figure 5: Examples of cluster profiles of a simulated photon (a) and simulated π^0 photons (b). The pads or pixels are 1 cm x 1 cm. The colours indicate the number of hits per pad. The single photon cluster is more circular than the π^0 photon cluster.

If two photons get too close, the identification of the two clusters will become problematic, since the clusters are merged into one (bigger) cluster. An example of such a merged cluster is shown in Fig. 5b. At low π^0 energy (up to 100 GeV) the profile of the decay photons per segment in the detector will form two non-overlapping circles and the FoCal clustering algorithm can easily identify both clusters (the clustering algorithm can identify both photons very well until the distance between the photons is about 1 cm). At high π^0 energy ($>$ 100 GeV), the two decay photons will hit the detector close to each other, so that the two clusters will be merged into a bigger cluster. In this case one can imagine that the merged cluster will start to look more like an elliptoid. To further clarify this, Fig. 6 is shown.

The σ_1 and σ_2 in Fig. 6 are the semi-major and the semi-minor widths respectively. In Fig. 6a the widths are the same, because a circle has only one radius. In Fig. 6b the two overlapping circles start to look like an ellipse with $\sigma_1 > \sigma_2$. On top of that the semi-minor axis σ_2 of single photon clusters should be equal or larger than the semi-minor axis of merged π^0 photon clusters.

As explained in Sec. 3.2, pixels will be rejected as a seed if they are within a certain area of a maximum in the energy. In order to discriminate between two photons that are close together and single photons, we can use the cluster shape method. This consists of comparing the semi-major σ_1 and the semi-minor σ_2 widths of the cluster. For a circle (single photon), σ_1 should equal σ_2, but for an ellipse (π^0 decay photons that are close together) $\sigma_1 > \sigma_2$.

The idea of the following simulations is to reproduce realistic clusters and analyze them to understand what the effect of different weights is on the cluster reconstruction. Also, the cluster shape method disciminating power varies accordingly with the function used to reproduce the cluster shape. The function that is used to reproduce the cluster shapes will be described in Sec. 4.1.

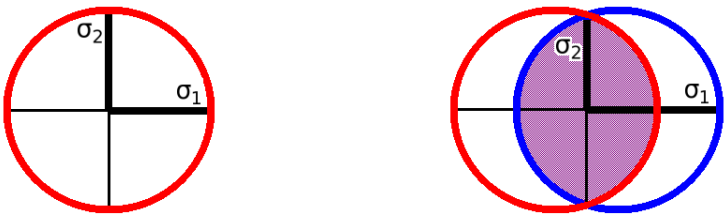

(a) Single photon cluster. (b) Merged π^0 photon clusters.

Figure 6: Single photon and π^0 photon clusters. The red and blue colours are the clusters of single photons. The purple colour shows the part of two clusters that overlaps, which can happen for high energy π^0 decay.

4.1 Double exponential

To create a cluster, that follows the profile of a cluster generated in a calorimeter, a *double exponential* distribution is used, which is suggested in [5]:

$$\frac{1}{r}\frac{dE}{dr} = \left(\alpha e^{-\frac{r}{c_0}} + \beta e^{-\frac{r}{c_1}}\right) , \tag{12}$$

with α and β free parameters. The double exponential gives the energy deposition at a radius r from the cluster center. Eq. (13) is the distribution used in the photon simulations in this research and is similar to the one proposed in the article.

$$\frac{1}{r}\frac{dE}{dr} = A\left(e^{-\frac{r}{c_0}} + Be^{-\frac{r}{c_1}}\right) , \tag{13}$$

with r is the radial distance, A and B free parameters, c_0 the Molière radius and c_1 the range of low energetic photons. The effective Molière radius of the FoCal is around 1 cm, therefore the parameter c_0 is set to 1 cm. From a fit of the data from the second coarse segment of the FoCal, the initial values in Table 1 were obtained. When generating clusters by using these parameters, only about 80% of the deposited energy (hits) is within 1 cm from the center of the cluster. This conflicts with the idea that 90% of the deposited energy should be within the Molière radius (which was set to 1 cm). Therefore a change was made to the fitted parameters. By using the initial conditions in Table 1 and an iterative process, the values in the last column of the table were obtained. With this iterative process, c_0 and A were taken constant (because c_0 is the Molière radius and A is just a scaling factor) and c_1 and B were changed, until the deposited energy within 1 cm of the center reached 90%. The distribution resulting from the obtained values is shown in Fig. 7. Note that the adjusted parameters have some degree of arbitrariness, since the same deposited energy might be achieved using a different set of parameters.

parameters	initial	adjusted
c_0	1.00	1.00
c_1	0.31	0.20
A	0.01	0.01
B	103.00	280.00

Table 1: Parameters used for the double exponential. The first column shows the parameter names. The second column shows the initial values for the parameters and the last column shows the parameter values obtained with the iterative process.

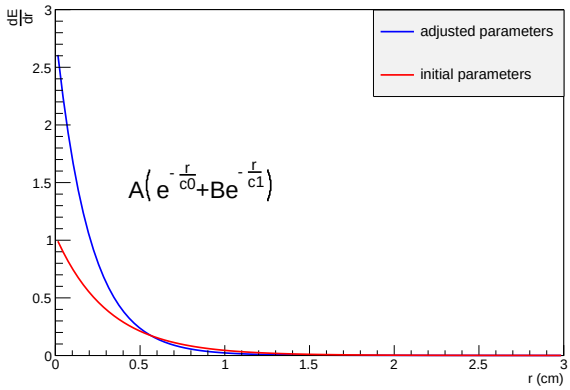

Figure 7: Double exponential function plotted for initial and adjusted parameter values.

4.2 Data generation

For this research clusters are generated and analysed. A cluster is made up of pads and each pad is hit a certain number of times. This amount corresponds to the amount of energy deposited in the pad. In this research the generated clusters are composed of 5000 hits. Because the total energy of a cluster is directly related to the number of hits, we can define the total energy of each cluster at the dimensionless value of 5000. This value corresponds to a deposited energy of a 500 GeV photon in the second coarse layer in the FoCal simulations. The clusters of the π^0 photons will overlap to create a combined cluster. The clusters are simulated in a way that the combined clusters also have an energy of 5000.

In the following sections, first the generation of single photon clusters will be explained, then the generation of the π^0 photon clusters. For each single photon cluster a center will be generated and then the cluster will be filled with hits or points. For π^0 photon clusters, two clusters that overlap have to be made in order to form a combined cluster. To do so, two centers, which are close together, need to be generated. Then the energy per cluster is generated and both clusters are filled with points around their center according to their energy. The clusters used for this research were filled with random points weighed with the distribution in Eq. (13). This cluster data is then projected onto a square grid, of -10 cm to 10 cm with pads of 1 cm x 1 cm. These pads only count the amount of hits and have no way of recording the exact position of a particular hit. This way position is only recorded in the position of the pad, which is a rough estimate of the position.

4.2.1 Single photon clusters

For single photon clusters, a random coordinate (x_{mean}, y_{mean}) for the center of the cluster is generated, with x_{mean} and y_{mean} both uniform between -1 cm and 1 cm. The cluster is then filled with points as follows: 5000 radii were drawn from the double exponential distribution and matched with 5000 random angles uniform in φ, with $\varphi \in [0, 2\pi]$. Now there are 5000 (r, φ) pairs, which are then transformed to 5000 (x, y) pairs. The coordinates of the center are added to these pairs. So in the end we have 5000 $(x + x_{mean}, y + y_{mean})$ pairs. Fig. 5 shows an example of data obtained in the way described above.

4.2.2 π^0 photon clusters

For π^0 creation, two clusters of photons have to be made. The first photon cluster is created in almost the same way as described above: first the center coordinate $(x_{mean,1}, y_{mean,1})$ is randomly generated, with $x_{mean,1}$ and $y_{mean,1}$ both uniform between -1 cm and 1 cm. As explained above the total energy of the combined cluster is 5000. Since there are two clusters, the total energy has to be devided amongst them. The energy E_1 for the first photon cluster is randomly generated, uniform between 2500 and 5000. The second cluster will have an energy $E_2 = 5000 - E_1$. This

way, the first cluster always has the highest energy of the two clusters. The energy asymmetry α is then defined as:

$$\alpha = \frac{E_1 - E_2}{E_1 + E_2} \,. \tag{14}$$

Now the distance between the two clusters has to be determined, which is done using the following equation:

$$d = \frac{c}{E\sqrt{1-\alpha^2}} \,, \tag{15}$$

with E the total energy of the combined cluster (set to 5000 in this research) and c a constant dependant on the total cluster energy and the minimum distance between the two clusters; if α is minimal, the distance is also minimal, therefore $d_{min} = \frac{c}{E}$, so $c = E\, d_{min}$. In this research d_{min} is set to 0.5 cm and this will be the minimal distance between the centers of the generated π_0 photon clusters. Therefore $c = 5000 * 0.5$ cm $= 2500$ cm. Now we only need an angle to obtain the location of the second cluster. The angle is again a random number uniform in φ, with $\varphi \in [0, 2\pi]$. Then the location of the second cluster is calculated by adding the (d, φ) pair to the $(x_{mean,1}, y_{mean,1})$ pair, which yields an $(x_{mean,2}, y_{mean,2})$ pair.

The number of hits per cluster and the locations have been set, so now the clusters need to be filled with random points. This is done the same way as with single photon clusters: using the double exponential function. The only difference is that there are now two clusters to be filled, with a different amount of hits around two different centers.

4.3 Clustering

In this section the equations for the analysis of the simulations for this research will be given.

4.3.1 Clustering equations

To find a measure for the widths of a cluster, the equations below are used. To begin with, it is necessary to find the shower center, which is an average in x and in y weighted with w_i. The weights w_i are based on the amount of energy deposited per cell in a cluster. There are multiple ways to calculate these weigths, which will be explained in the sections below. The cluster center positions are calculated:

$$\begin{aligned} \langle x \rangle &= \frac{\sum w_i x_i}{\sum w_i} & \qquad \langle x^2 \rangle &= \frac{\sum w_i x_i^2}{\sum w_i} \\ \langle y \rangle &= \frac{\sum w_i x_i}{\sum w_i} & \qquad \langle y^2 \rangle &= \frac{\sum w_i x_i^2}{\sum w_i} \\ \langle xy \rangle &= \frac{\sum w_i x_i y_i}{\sum w_i} \end{aligned} \tag{16}$$

Then the variances and covariances need to be calculated:

$$\begin{aligned} \sigma_{x^2} &= \langle x^2 \rangle - \langle x \rangle^2 \\ \sigma_{y^2} &= \langle y^2 \rangle - \langle y \rangle^2 \\ \sigma_{xy} &= \langle xy \rangle - \langle x \rangle \langle y \rangle \,. \end{aligned} \tag{17}$$

Now the equations for finding the widths [4]:

$$\begin{aligned} d_{\sigma_x \sigma_y} &= \sigma_{y^2} - \sigma_{x^2} & \qquad \sigma_1 &= \sqrt{\frac{\sigma_{x^2} + \sigma_{y^2} + s}{2}} \\ s &= \sqrt{d^2_{\sigma_x \sigma_y} + 4(\sigma_{xy})^2} & \qquad \sigma_2 &= \sqrt{\frac{\sigma_{x^2} + \sigma_{y^2} - s}{2}} \,. \end{aligned}$$

The reconstructed cluster will have σ_1 and σ_2 as a measure of the widths of the cluster. σ_1 is the semi-major axis and σ_2 is the semi-minor axis as can be seen in Fig. 8. The following equation is used to obtain the orientation of the reconstructed cluster.

$$\varphi = \arctan\left(\frac{(d_{\sigma_x\sigma_y} + s)\langle y\rangle + 2\sigma_{xy}\langle x\rangle}{2\sigma_{xy}\langle y\rangle - (d_{\sigma_x\sigma_y} - s)\langle x\rangle}\right), \qquad \text{with } \varphi \in \left[-\frac{\pi}{2}, \frac{\pi}{2}\right]$$

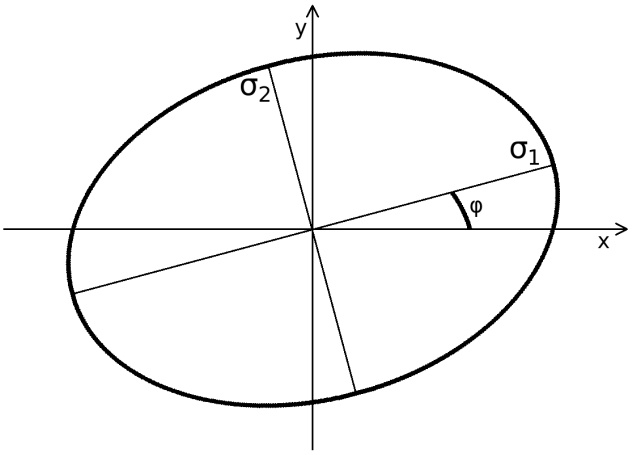

Figure 8: Ellipse, with σ_1 and σ_2 the semi-major and semi-minor axes respectively and φ the angle with the horizontal axis.

4.3.2 Linear weighting

To reconstruct the cluster widths in the previous section, we need to take the deposited energy per cell into account. The normal way to do this, is by using linear weights:

$$w_i = \frac{E_i}{E_T}\,, \tag{18}$$

with w_i the weight in the i^{th} cell, E_i the deposited energy in the i^{th} cell and E_T the total deposited energy in all the cells of the cluster.

4.3.3 Logarithmic weighting

Instead of using linear weighting for electromagnetic showers, it is suggested to use logarithmic weighting [6]:

$$w_i = \max\left\{0, \left[w_0 + \ln\left(\frac{E_i}{E_T}\right)\right]\right\}\,, \tag{19}$$

with w_0 a free parameter. This logarithmic weighting is introduced to enhance the influence of the tail of a cluster, which is useful to reconstruct the found clusters better. The free parameter w_0 is needed to compensate for the effect that the logarithm is always smaller than 0, because the argument of the logarithm ($\frac{E_i}{E_T}$) is always smaller than 1. It is nescesary to optimize w_0; if w_0 is too low, a big part of the tail is cut off, and if w_0 is too high, the tail contributes to much, which makes statistical fluctuations to have a larger effect. Fig. 9 shows $\frac{E_i}{E_T}$ and $w_0 + \ln\left(\frac{E_i}{E_T}\right)$ plotted for different values of w_0; as can be seen, w_i rises more rapidly at small $\frac{E_i}{E_T} < 0.1$ for larger w_0.

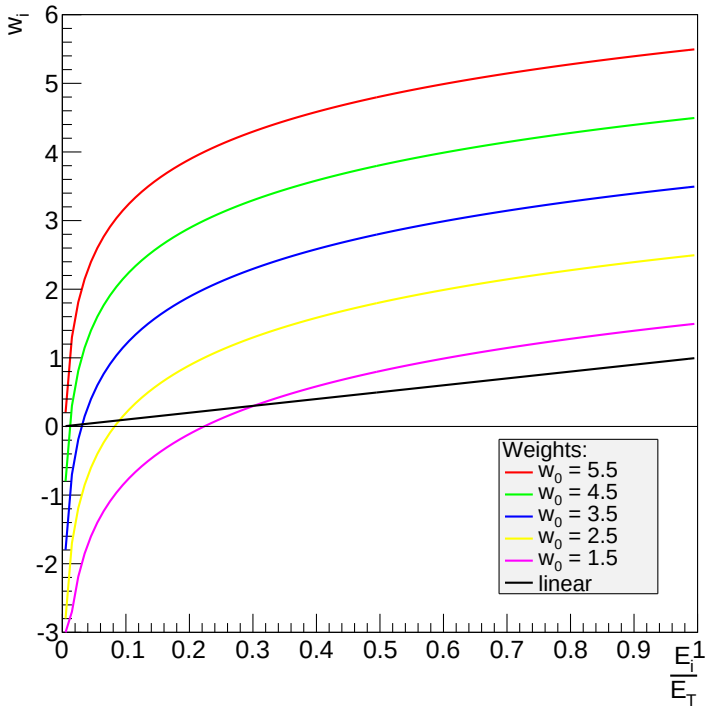

Figure 9: Linear and logarithmic weighting with different w_0.

4.4 Method of data analysis

Each set of data contains 10000 clusters and each cluster spans a certain amount of pads and these pads contain a number of hits. The number of hits per pad needs to be interpreted in a way that the clusters properties, such as location and widths, are reconstructed the best. There are different ways to analyze the data obtained as described in Sec. 4.2. For each set of data, different weights are used. The different weights influence the way the properties of the clusters are reconstructed. First, linear weighting was used and then logarithmic weighting, for 27 different w_0, which resulted in a total of 28 different weights and thus 28 different sets of data. Now, the first thing we want to know is how the *hit locations* of the clusters are reconstructed. The hit location of a cluster is defined as the center of the cluster. When the best weighting is used, the reconstructed hit location will be closest to the original constructed center (x_{mean}, y_{mean}) of the cluster. After the reconstruction of the hit locations, the widths of the clusters will be calculated. In the end we want to obtain an optimized weight w_i (linear or logarithmic, with the best w_0) in order to discriminate between single photon clusters and π^0 photon clusters.

4.4.1 Method of hit location reconstruction

As explained in Sec. 4.2.1 the cluster centers are generated uniformly between -1 cm and 1 cm in x and y. Thus, the surface where the centers are generated spans 2x2 pads. As the generated hit locations are uniformly distributed, ideally the reconstructed hit locations must also be uniform. To evaluate the uniformity of the reconstructed hit locations, two steps must be undertaken: first, the integer part is subtracted from the coordinates, so we only have the fractional parts $\{x\}$ and $\{y\}$ left. This step ensures that all the reconstructed hit locations are within 0 and 1 cm in x and y, so effectively they are all placed on a single 1 cm x 1 cm pad. Second, all the 10000 fractional reconstructed hit locations are plotted on top of each other on a 1 cm x 1 cm pad, creating a two dimensional histogram.

This hit location reconstruction will only be done for single photon clusters and not for π^0 photon clusters. It is not useful to look at reconstructed hit locations for π^0 photons, since the

hit location of such a cluster does not resemble anything. The cluster finding algorithm would in this case not be able to identify the two photons, therefore the widths should say something about those clusters.

4.4.2 Method of widths reconstruction

So after the hit location reconstruction we have a certain optimized weight parameter for single photon clusters. Now we want to to distinguish between single photon clusters and π^0 photons clusters. The single photon clusters are generated in a way that the outline should form a circle. Therefore σ_1 should equal σ_2, however due to statistical fluctuations this will never really be the case. The π^0 photon clusters are generated with a small distance between them. As explained above, these clusters in general should have larger σ_1 than single photon clusters and the σ_2 should be more or less equal to the σ_2 of single photon clusters. To see the difference, the widths of the single photon clusters and of the π^0 photon clusters will be plotted in a single figure. This will again be done for multiple weights, to check what weight yields the best discriminating power.

5 Results

The results of the simulations will be presented in the following sections.

5.1 Hit location reconstruction

One of the goals of this research was to find out how the hit locations were reconstructed for different weights. This has been done only for single photon clusters as explained in Sec. 4.4.1. Fig. 10 gives a visualization of the hit location reconstruction. It shows the distribution of the reconstructed hit locations for four different weights: linear and logarithmic, with $w_0 \in [4.5, 5.3, 5.8]$. The colours represent the number of hits per bin and on the x- and y-axes, $\{x\}$ and $\{y\}$ are plotted, which are the fractional parts of x and y respectively. The figure shows some noticable features: the first two distributions have a dense center and dense corners respectively, while the last two are much more uniform. Appearantly the linear weighting does not reconstruct the hit locations uniformly across the pad and neither does the logarithmic weighting with $w_0 = 4.5$. By using higher w_0's of 5.3 and 5.8 the hit locations are reconstructed better in the sense that they at least return the uniformity of the original distributions.

In order to have the real hit locations reconstructed the best, the distance between the real hit locations and the reconstructed hit locations should be small. To get a feeling of how good the algorithm reconstructs the hit location as a function of w_0, the difference between the reconstructed hit locations and the generated hit locations is shown in Fig. 11. The figure has the following main features: the first two distributions are more or less peaked to the right and the bins go up to about 0.14 cm. The last two distributions are peaked to the left and the bins hardly cross the 0.1 cm. This means that the logarithmic weighting with higher w_0's, the reconstructed hit locations are closest to the generated hit locations.

To further check at what value of w_0 the positions are reconstructed the best, Fig 12 is given. It shows the difference between the reconstructed x-position and the real x-position in red and the reconstructed y-position and the real y-position in blue of the reconstructed hit locations. This way of plotting the difference gives a root mean square (RMS) for the width of the distribution. Again, the lower this value of the RMS, the better the positions have been reconstructed. The distributions for x and y are almost identical and the RMS in the x-direction is the same as for the y-direction. To show how the RMS in the x-direction depends on the used weighting, Fig. 14 is given. The error bars are multiplied with a factor of 10 to make them visible.

Finally, the reconstructed x-position minus real x-position has been plotted against the real $\{x\}$-position in Fig. 13. The y-positions are not shown, since the profile would be the same as for the x-positions, which is made clear in Fig. 12. With linear weighting, the best reconstructed hit locations are at the center or the edge of a pad. The same goes for $w_0 = 4.5$, although across the pad in the x-direction there are some cases of good reconstructed positions. If $w_0 = 5.3$ or $w_0 = 5.8$ the profile is much smoother, but it is still visible that clusters created in the center of a pad are reconstructed the best.

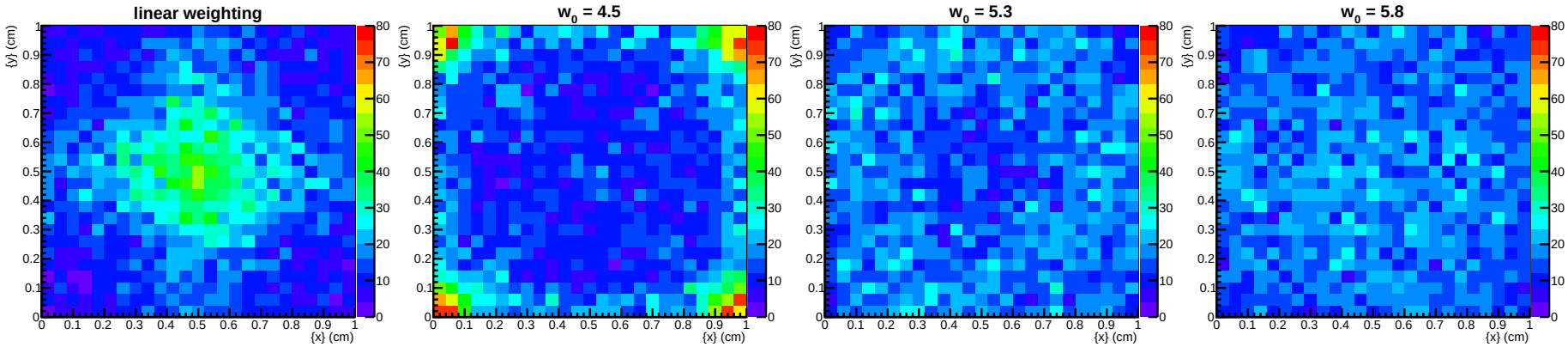

Figure 10: Reconstructed hit locations.

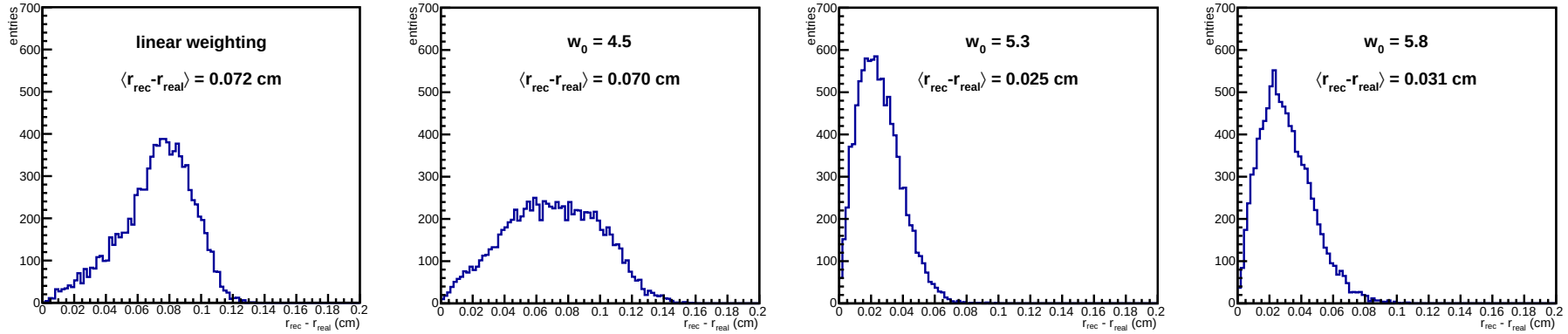

Figure 11: Distance between reconstructed and real position. The first two figures are relatively flat and peaked to the right, while the last two figures are peaked to the left.

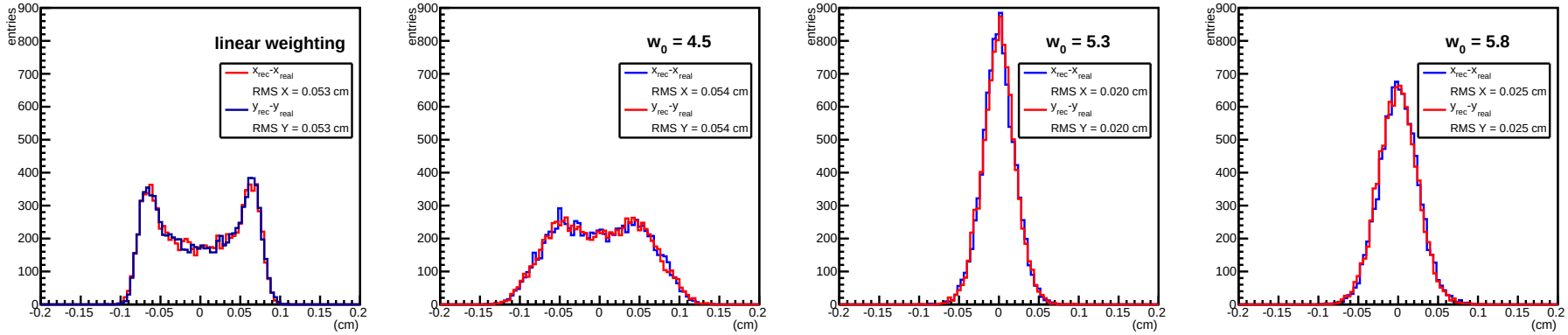

Figure 12: Reconstructed x-position - real x-position (blue) and reconstructed y-position - real y-position (red).

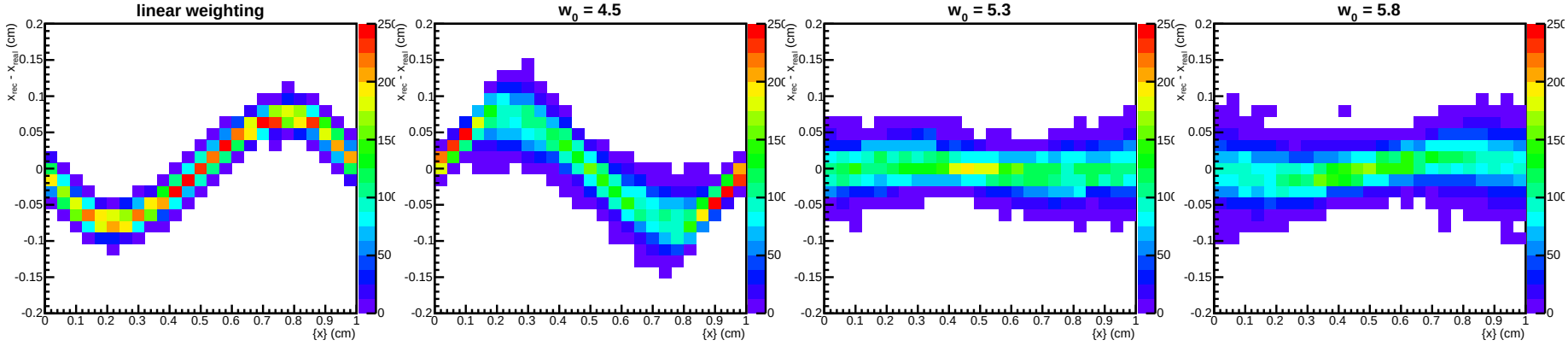

Figure 13: (Reconstructed x-position - real x-position) vs real fractional x.

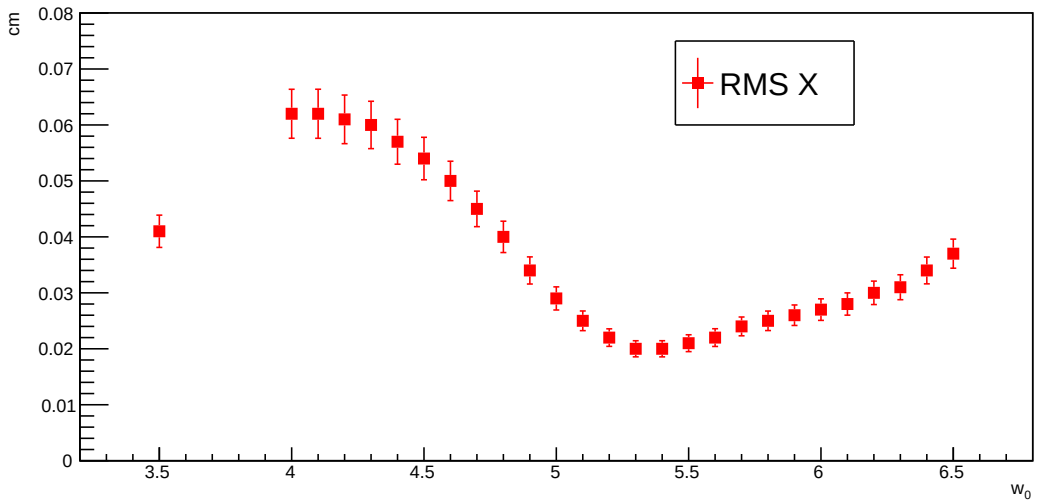

Figure 14: RMS X plotted vs w_0. The error bars are the errors on the RMS and they are multiplied by 10 to make them visible. The lowest RMS value is at about $w_0 = 5.3$.

5.2 Widths reconstruction

It is clear that in the single photon simulations, for most cases, logarithmic weighting performs better at reconstructing cluster positions than linear weighting. When combining the results from the four figures described above, the best value for the parameter $w_0 = 5.3$. The most interesting part is, however, to differentiate between single photons clusters and two photons clusters that are very close together.

Let us first take a look at the shape of single photon clusters for some different weights w_i in Fig. 15. With linear weighting there is a relatively large spread in σ_1 and σ_2. Also σ_2 is often a lot (0.1 to 0.2 cm) smaller than σ_1. When looking at the other three, there is a general rise in σ_1 and σ_2. This is due to the fact that as w_0 increases, the edge of a cluster has more effect on the cluster reconstruction. The distribution with $w_0 = 5.8$ seems to have the smallest spread in σ_1. The clusters reconstructed with $w_0 = 5.8$ have the most circular reconstructed shape, compared to the other values of w_0.

The shape of π^0 photon clusters is shown in Fig. 16. When comparing this figure with Fig. 15, it is clear that there is a larger spread in the semi-major axis σ_1 for π_0 photon clusters, while the spread in the semi-minor axis σ_2 remains more or less the same. This is to be expected, because the two photon clusters are in general more elliptic than the single photon clusters.

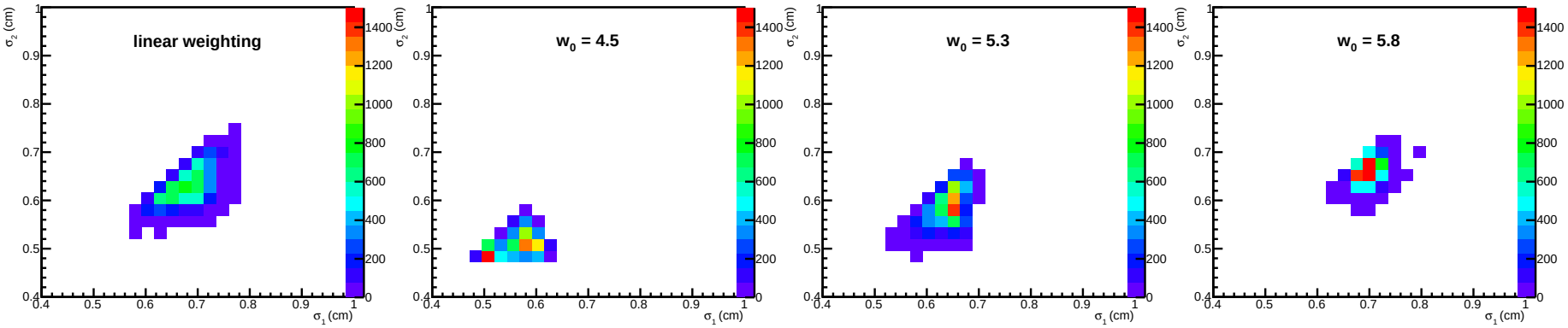

Figure 15: Single photon clusters: σ_2 vs σ_1 for different weights.

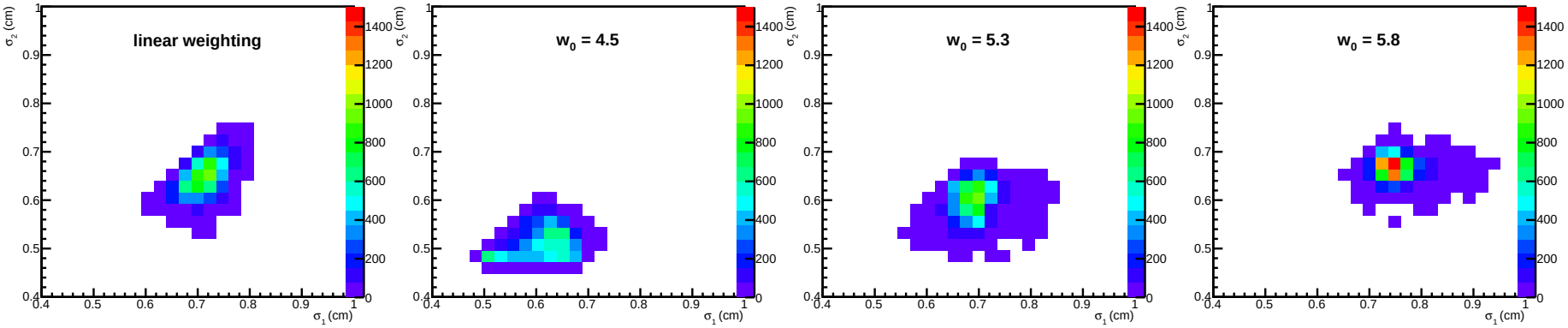

Figure 16: π^0 photon clusters: σ_2 vs σ_1 for different weights.

We now want to know how well the semi-major widths are separated and how the semi-minor widths overlap for different weights. Fig. 17 shows the normalized distributions of σ_1 and Fig. 18 shows the normalized distrbutions of σ_2 for single photon and π^0 photon clusters. The widths for the single photon clusters are blue and red for the π^0 photon clusters.

When one would place cuts on the σ_1 distributions to reject the π^0 photon clusters, the best result would be obtained with $w_0 = 5.8$. If for example the cut is placed at the point where the red and blue distributions intersect, only a minimal amount of π^0 photon clusters would be falsely considered as single photon clusters. On top of that only a small portion of the single photon clusters would be discarded. For the distributions with $w_0 = 5.3$ one would also obtain a good result, but for the other two distributions (linear and $w_0 = 4.5$), a lot of π^0 photon clusters and a lot of single photon clusters would be falsely taken and discarded respectively.

Let us now take a close look at Fig. 18. The distributions with $w_0 = 5.8$ overlap almost completely. Based on Fig. 6b this is what we would expect. Also the distribution with $w_0 = 4.5$ seems to have a good overlap. The distributions with linear weighting and $w_0 = 5.3$ show the smallest overlap.

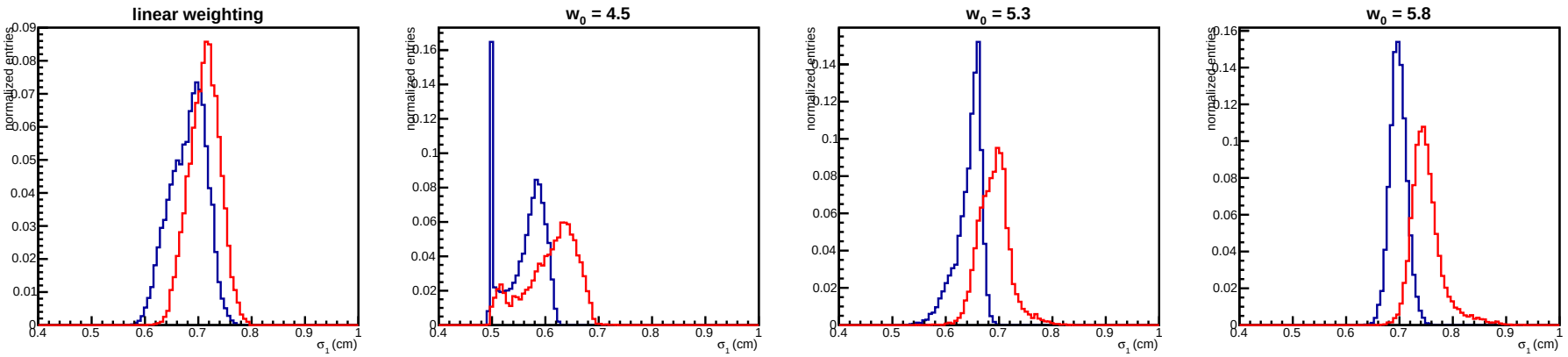

Figure 17: σ_1 for single photon clusters (blue) and π^0 clusters (red).

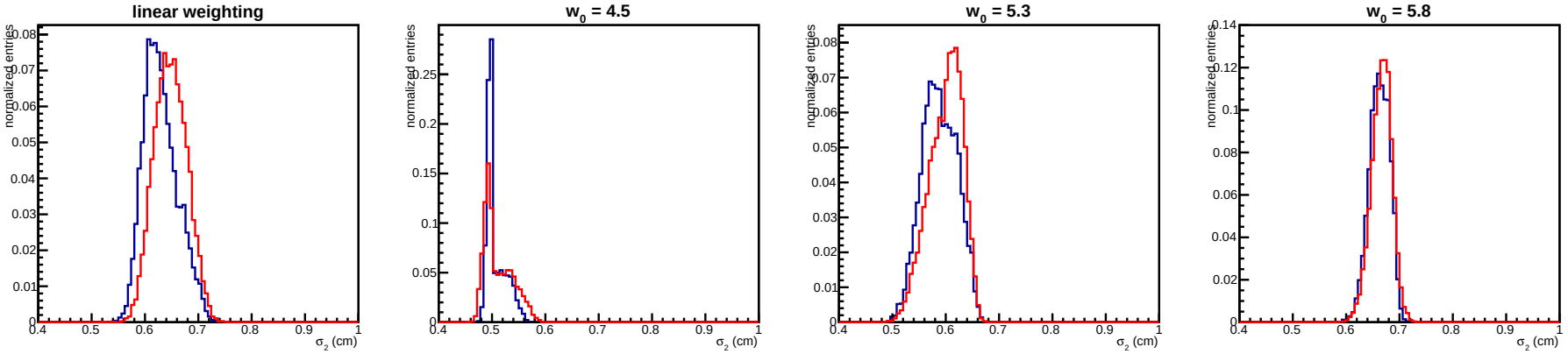

Figure 18: σ_2 for single photon clusters (blue) and π^0 clusters (red).

Based on Fig. 17 and 18, the best value for widths reconstruction would be $w_0 = 5.8$. To see what the widths do for a large w_0 region we can look at Fig. 19 and 20. The error bars are the standard deviations from distributions like the ones in Fig. 17 and 18. When inspecting the w_0 region from $5.6 \leq w_0 \leq 5.8$ in Fig. 19, the difference between the single photon clusters and π^0 photon clusters is largest and has the smallest error bars. When looking closely to Fig. 20 the σ_2 difference is smallest and has the smallest error bars in the region from $5.8 \leq w_0 \leq 6.0$. So both regimes have only one w_0 value that overlaps and that is $w_0 = 5.8$. Based on these two figures, $w_0 = 5.8$ would also seem the best parameter for widths reconstruction.

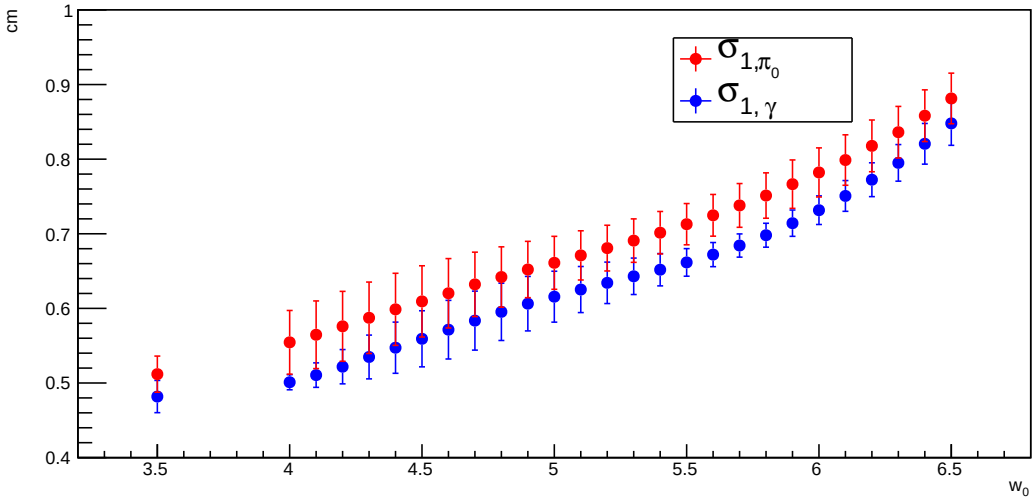

Figure 19: σ_1 for single photon clusters (blue) and π^0 photon clusters (red). The error bars are the standard deviations from distributions like in Fig. 17.

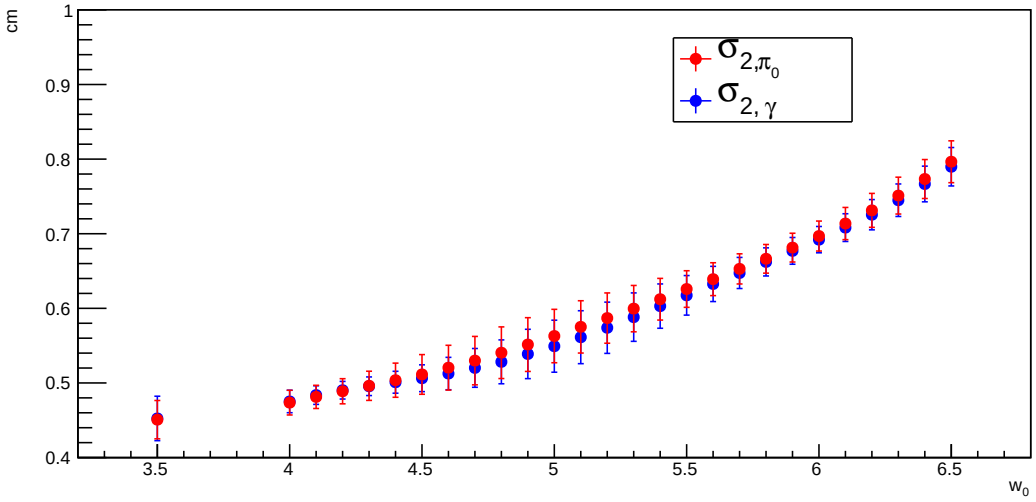

Figure 20: σ_2 for single photon clusters (blue) and π^0 photon clusters (red). The error bars are the standard deviations from distributions like in Fig. 18.

6 Discussion

The results of the simulations will be discussed and further research is presented.

6.1 Simulation results

The clusters that were simulated for this research were generated via a double exponential function, which was based on a fit of clusters from the second coarse segment in the FoCal. First, the hit locations for single photon clusters were reconstructed, which yielded the best results for logarithmic weighting with $w_0 = 5.3$. Then the single photon clusters and π^0 photon clusters were compared to each other by analyzing the widths of the clusters. For single photon clusters, $\sigma_1 = \sigma_2$ (in the perfect case) and for π^0 photon clusters, $\sigma_1 > \sigma_2$, which was best reconstructed with $w_0 = 5.8$. Finally, the width differences were presented, which gave different results: the separation of σ_1 was best for $5.6 \leq w_0 \leq 5.8$, but the overlapping of σ_2 was best for $5.8 \leq w_0 \leq 6.0$.

This gives a small range of acceptable w_0 values, with the best value for width reconstruction of around $w_0 \backsimeq 5.8$. So there are two values of w_0 (5.3 and 5.8) that are the best for reconstructing cluster hit locations and cluster widths respectively. This research only focussed on the coarse segments of the FoCal, but the FoCal also has fine segments. These fine segments are able to do better hit location reconstruction, because the pixels are only 1 mm x 1 mm as opposed to 1 cm x 1 cm pads in the coarse segments. Seemingly the best solution would be to reconstruct the hit locations using the fine segments and the width reconstruction with the coarse segments. Therefore the best value of w_0 for the simulations in this research would be $w_0 \backsimeq 5.8$.

6.2 Further reasearch

In this research only clusters of 5000 hits have been considered. To get a better view of the behaviour of the logarithmic weighting, other energy regimes need to be researched as well. On top of that, the results from the simulations cannot directly be used to improve the FoCal, but what it does show is that for some cases logarithmic weighting performs a lot better than linear weighting. And that there is a certain range of w_0 values for which the cluster reconstruction is done best.

Also, not only direct photons and photons from π^0 decay will be measured by FoCal. Therefore it is useful to know what the effect of logarithmic weighting will be on the reconstruction of the other particles. There is a whole lot of research to be done before the actual measurements of the real FoCal can provide data of elementary particles in collisions.

7 Acknowledgements

I would like to thank my supervisor Dr. Ir. M. van Leeuwen and my co-supervisors Drs. D. Lodato and Drs. A. Babeanu, who helped me understand the physics involved in my research and gave me extra time I needed involving recent events. I would like to thank the rest of the FoCal group for their questions during the wednesday presentations, which for me led to a better understanding of the problems. Also I would like to thank Prof. Dr. T. Peitzmann for the final remarks on my thesis. Finally I want to thank K. Sponselee and T. Bannink for their views and ideas and the debugging of my code.

References

[1] The alice experiment at lhc. URL http://www.phy.ornl.gov/groups/heavy_ions/ALICE.html.

[2] The ALICE FoCal Collaboration. Letter of intent: A forward calorimeter (focal) for the alice experiment. *EUROPEAN ORGANIZATION FOR NUCLEAR RESEARCH*, 02 2013.

[3] J. Beringer et al. Review of particle physics. *Physical Review D*, 86, 06 2012. URL http://pdg.lbl.gov.

[4] David J. Fegan. γ/hadron separation at tev energies. *Journal of Physics G: Nuclear and Particle Physics*, 23(9), 09 1997.

[5] H.-C. Schultz-Coulon and J. Stachel. Calorimetry i. *Lecture & Journal Club*, 06 2011. URL http://www.kip.uni-heidelberg.de/~coulon/Lectures/Detectors/Free_PDFs/Lecture9.pdf.

[6] Awes-F. E. Obenshain F. Plasil S. Saini S.P. Sorensen T, C. A simple method of shower localization and identification in laterally segmented calorimeters. *Elsevier*, 311, 01 1992.